

MonoTDP: Twin Depth Perception for Monocular 3D Object Detection in Adverse Scenes

Xingyuan Li
xingyuan_lxy@163.com
Dalian University of Technology
Dalian, Liaoning, China

Jingyuan Liu
atlantis918@hotmail.com
Dalian University of Technology
Dalian, Liaoning, China

Yixin Lei
yixinlei121@gmail.com
Dalian University of Technology
Dalian, Liaoning, China

Long Ma
longma@mail.dlut.edu.cn
Dalian University of Technology
Dalian, Liaoning, China

Xin Fan
xin.fan@dlut.edu.cn
Dalian University of Technology
Dalian, Liaoning, China

Risheng Liu
rslu@dlut.edu.cn
Dalian University of Technology
Dalian, Liaoning, China

ABSTRACT

3D object detection plays a crucial role in numerous intelligent vision systems. Detection in the open world inevitably encounters various adverse scenes, such as dense fog, heavy rain, and low light conditions. Although existing efforts primarily focus on diversifying network architecture or training schemes, resulting in significant progress in 3D object detection, most of these learnable modules fail in adverse scenes, thereby hindering detection performance. To address this issue, this paper proposes a monocular 3D detection model designed to perceive twin depth in adverse scenes, termed MonoTDP, which effectively mitigates the degradation of detection performance in various harsh environments. Specifically, we first introduce an adaptive learning strategy to aid the model in handling uncontrollable weather conditions, significantly resisting degradation caused by various degrading factors. Then, to address the depth/content loss in adverse regions, we propose a novel twin depth perception module that simultaneously estimates scene and object depth, enabling the integration of scene-level features and object-level features. Additionally, we assemble a new adverse 3D object detection dataset encompassing a wide range of challenging scenes, including rainy, foggy, and low light weather conditions, with each type of scene containing 7,481 images. Experimental results demonstrate that our proposed method outperforms current state-of-the-art approaches by an average of 3.12% in terms of AP_{R40} for car category across various adverse environments.

CCS CONCEPTS

• Computing methodologies → Computer vision.

KEYWORDS

3D object detection, monocular vision, image enhancement

1 INTRODUCTION

In general, vision-based object detection plays a critical role in autonomous driving and infrastructure-independent robot navigation. These detection techniques are employed to interpret the surrounding environment by recognizing and categorizing object instances,

as well as determining their spatial positions and orientations. Although recent advances in 2D object detection[7, 53] have shown significant improvements in both accuracy and processing speed, 3D object detection remains a more complex task, as it strives to simultaneously determine the pose and location of each object.

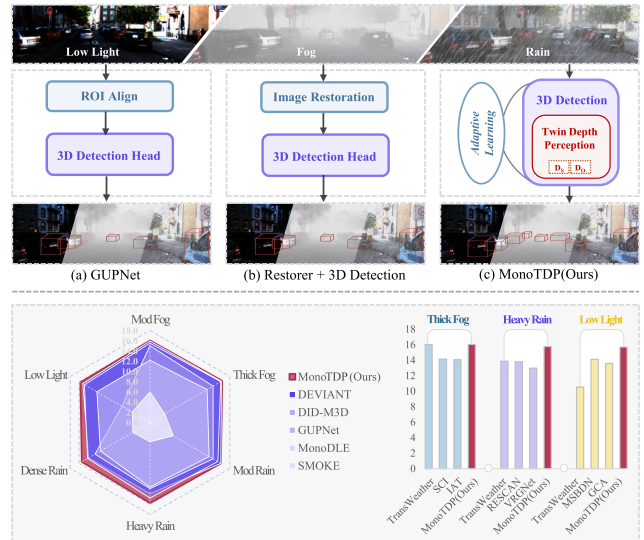


Figure 1: The top row illustrates 3D object detection methods in adverse scenes: (a) existing models overlooking environmental context, causing errors; (b) conventional solutions using image restoration, potentially yielding unsuitable images; (c) Our MonoTDP method that employs adaptive learning strategy to acclimate to harsh weather by penalizing perceptual errors and improving instance depth estimation via perceiving scene depth. The bottom row showcases the performance comparison, revealing MonoTDP’s superior average precision across all six weather conditions, highlighting its significant performance enhancement.

A common approach to 3D object detection frequently involves the use of LiDAR sensors or stereo cameras for depth estimation[34, 41, 42, 52]. Although these methods can provide accurate depth information, they significantly increase the cost of implementing practical systems. Consequently, monocular 3D object detection[4,

26] has emerged as a promising alternative, garnering considerable interest within the research community.

Over the past few years, numerous monocular 3D object detection techniques have been proposed and successfully implemented. These approaches can be broadly classified into two categories: those based on single images [1, 26] and those leveraging auxiliary information [27, 40]. Single-image based techniques, such as M3D-RPN[1] and MonoDLE[26], primarily focus on extracting depth information from a single input image. They employ innovative strategies like depth-aware convolution and depth error analysis to enhance detection performance, offering cost-effectiveness and simplicity in the process. On the other hand, auxiliary-information based methods, including RoI-10D[27] and Pseudo-LiDAR[40], incorporate supplementary data sources, such as CAD models or point clouds, to enrich the detection process. This additional information helps to overcome the limitations inherent in single-image based approaches, leading to more robust and accurate object localization and classification. Collectively, these methodologies have significantly advanced the field of 3D object detection, enabling more accurate and reliable object localization and classification in various application scenarios.

Nevertheless, these methods have encountered several issues, primarily in the following three aspects. (i) 3D object detection is inevitable to face real-world adverse conditions, such as rain occlusions, fog-induced scattering, and texture loss in low-light situations. These conditions lead to degraded image quality, partial or complete occlusion of objects, blurring effects, and reduced contrast, ultimately undermining the detection performance. (ii) Monocular 3D detection is inherently limited by the single viewpoint, making it difficult to recover depth information from a single 2D image, as the camera projection process results in the loss of spatial information. This limitation can lead to ambiguities and uncertainties in depth estimation, posing challenges for accurate object localization and classification. (iii) The scarcity of datasets hinders advancements in the field. There is a lack of comprehensive datasets capturing a wide range of adverse weather conditions and complex environments characteristic of real-world driving scenarios. This deficiency restricts the learning of complementary information and validation of detection algorithm effectiveness, thus impeding progress in developing more robust and adaptable 3D object detection techniques.

To address the aforementioned issues, we propose a novel monocular 3D object detection method tailored for challenging environments, dubbed MonoTDP. Our approach incorporates an adaptive learning strategy and a twin depth perception module. The adaptive learning strategy, during training, penalizes incorrect perception of harsh conditions, fostering robust multi-environment capabilities. This allows our method to better adapt to complex scenarios, such as rain, fog, and low light. The twin depth perception module tackles depth ambiguity by estimating both scene and object depth using scene-level and object-level features, effectively recovering missing depth cues in degraded regions. We introduce a diverse dataset covering various challenging scenarios, including moderate fog, thick fog, dense fog, moderate rain, heavy rain, dense rain, and low light conditions. Each category consists of 7,481 images. Figure

1 demonstrates that our proposed model outperforms state-of-the-art(SOTA) 3D object detectors and cascade of image enhancement and 3D detection models. Our contributions are four-fold:

- We introduce a robust network specifically designed to handle a variety of adverse environments, significantly improving the performance and resilience of monocular 3D object detection models across a wide range of challenging real-world situation.
- We propose an adaptive learning strategy implemented during the training process, enabling the model to acclimatize to inclement weather conditions and augment the precision of 3D object detection. This component aids the model in discerning various environments and extracting resilient features that remain less susceptible to degrading factors.
- A twin depth perception module is incorporated to address the challenge of depth estimation in adverse settings by concurrently leveraging object-level features for object depth estimation and scene-level features for scene depth estimation. This approach mitigates the problem of information and depth loss under diverse unfavorable conditions.
- To support 3D object detection in harsh environments, we have compiled a comprehensive dataset comprising 7,481 images for each of the seven demanding conditions: moderate fog, thick fog, dense fog, moderate rain, heavy rain, torrential rain, and low light.

2 RELATED WORK

2.1 Monocular 3D Object Detection

Monocular 3D object detection can be roughly divided into single-image based methods and auxiliary-information based methods.

The most commonly used methods take only one image as input and output the 3D information of the object in the image. To estimate the depth, M3D-RPN[1] designed a depth-aware convolution that can better obtain 3D area proposals to perceive depth information. For the simplicity and effectiveness of the model, SMOKE[22] and FCOS3D[39] proposed a one-stage monocular 3D detection model based on CenterNet[5] and FCOS[36] respectively. MonoDLE[26] obtained more reliable results by analyzing the manually designed depth error. MonoFLEX[50] used uncertainty-guided depth and adopted special treatments for different objectives.

Plenty of approaches use additional data to assist the learning of monocular 3D detection models. RoI-10D[27] used CAD models to introduce prior knowledge to enhance training samples. Pseudo-LiDAR[40] proposed to lift the estimated depth to the point cloud and then use a detector based on the LiDAR method. DID-M3D[29] used a dense depth map. However, the previous works do not consider the impact of complex environments. Thus, we design a model that can adapt to various adverse scenes.

2.2 Degradation Factor Removal

It has been widely explored to remove degradation factors from images in adverse weathers, such as rain removal[12, 18, 19, 37, 43], fog removal[2, 11, 16, 20, 46], low-light enhancement[3, 14, 15, 17, 21, 44, 51].

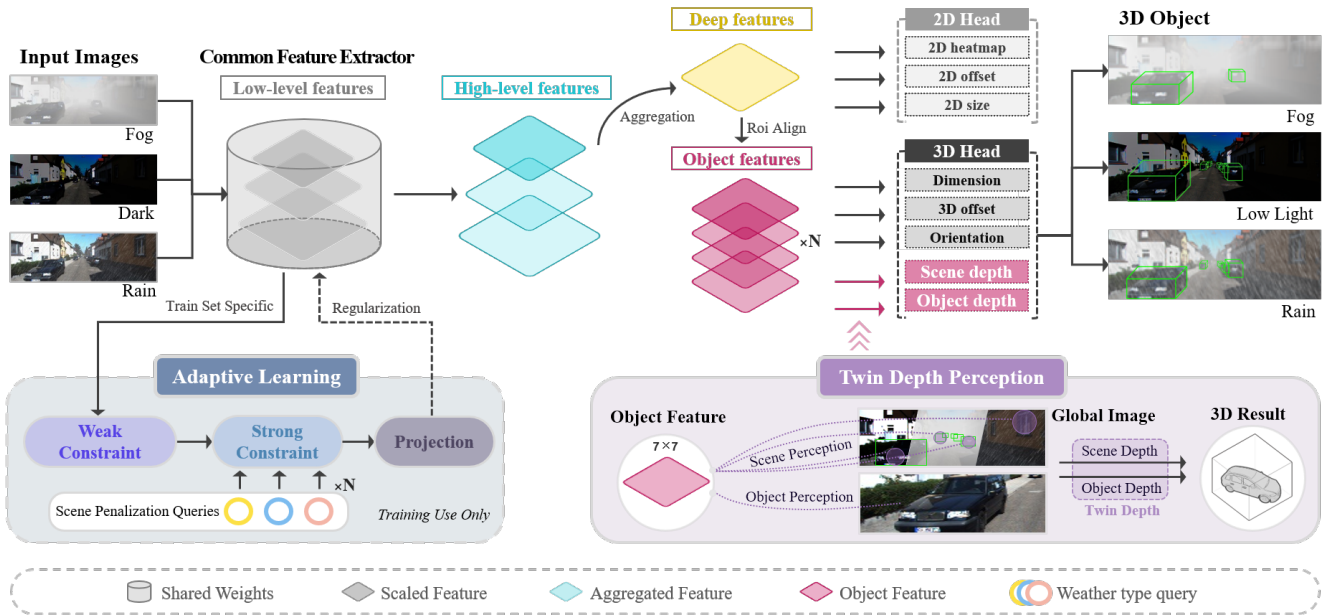


Figure 2: The pipeline of MonoTDP. It consists of two core components: Adaptive Learning (Sec. 3.2) regularizes features from Common Feature Extractor to help model perceive clean meta features that are not degraded by adverse factors, and it is only used in training stage. Twin depth perception module (Sec. 3.3) is conducted in 3D object detection under adverse weather conditions to obtain better instance depth by combining scene depth and object depth.

To remove rain, [43] split the rain streak into different layers, [47] used a GAN-based method and [30] used a dual attention mechanism. To cope with haze, DehazeNet[2] restored the visibility of images through a scattering transformation. DCPDN[45] generated transmission map, atmospheric light and dehazing map. [48] designed a hierarchical dense perceptual network. To enhance low-light, LLNet[23] adaptively brightened images through multi-layer encoders. [25, 32, 33, 35] used multi-scale features to better restore clear images. [33] used two deep networks to decouple images.

Furthermore, there are some all-in-one[12] networks. [12] used multiple discriminative encoders to deal with different environments. U-former[38], Swin-IR[13] proposed to solve image restoration problems in adverse environments based on different Transformers. Different from them, the method we proposed can both handle multiple adverse scenes and benefit 3D object detection through an adaptive learning strategy.

2.3 Depth Estimation

There are also methods that utilize geometric constraints and scene priors to use auxiliary data to help depth estimation. The early work [28] used 2D-3D box geometric constraints to estimate instance depth. But this indirect approach which does not fully use of supervisions has poor performance. [9] predicted nine perspective key-points of a 3D bounding box in the image space and optimized the initially estimated instance depth by minimizing projection errors. [8] followed this line and integrated this optimization into an end-to-end training process. Recently, [50] predicted the nine-perspective key-points and produced new instance depths by using

the projection heights in pair key-points and geometric relationships.

In this paper, we propose a 3D object detection model facing adverse scenes that can benefit from twin depth perception and adaptive learning strategy.

3 METHOD

Under various inclement weather conditions, the specific spectral interaction between captured objects and the camera may be affected by the absorption and scattering caused by suspended water droplets, dust, and other particulates, resulting in the loss of depth information for 3D object detection. To address this challenge, we present a monocular 3D object detection model, namely MonoTDP, for adverse environments. As depicted in Figure 2, images undergo processing via a shared feature extractor, which constitutes a part of the 2D detection backbone and is guided by the adaptive learning strategy which effectively mitigates the interference caused by various degrading factors. Consequently, we obtain deep features, 2D bounding boxes, and fundamental 3D bounding box information, such as dimensions, 3D projected centers, and angles. Subsequently, the twin depth perception module simultaneously predicts scene depth and object depth. The integration of scene depth and object depth yields accurate inferred depth values under different degrees of challenging conditions, facilitated by the comprehensive interaction between scene-level and object-level features.

3.1 Adverse Condition Datasets Generation

Currently, there is a significant shortage of reliable 3D object detection datasets specifically designed for adverse weather conditions.

To address this issue, we have compiled datasets encompassing a wide range of adverse weather conditions, such as fog, rain, and low light, to conduct comprehensive experiments using our proposed approach, MonoTDP.

In the literature, various weather phenomena are modeled differently based on their underlying physical properties. The process of synthesizing adverse weather conditions is primarily based on the simulation of their corresponding atmospheric effects. According to the atmospheric light attenuation theory [49], the fog condition is modeled as:

$$\mathbf{I} = \mathbf{B} \odot \mathbf{T} + \mathbf{A} \odot (1 - \mathbf{T}), \quad (1)$$

where \mathbf{I} represents the degraded image, \mathbf{B} denotes the background, \mathbf{A} refers to the atmospheric light in the scene, and \mathbf{T} signifies the light propagation formula, which can be expressed as:

$$\mathbf{T} = e^{-\beta \mathbf{d}}, \quad (2)$$

where \mathbf{d} corresponds to the depth value of the image, and β is a variable to modulate the scattering effect. This model enables the accurate representation of foggy conditions by simulating the scattering of light particles due to the presence of fog.

Rain with rain streaks and fog effect [10] is modeled as:

$$\mathbf{I} = \mathbf{T} \odot \left(\mathbf{B} + \sum_i^n \mathbf{R}_i \right) + (1 - \mathbf{T}) \odot \mathbf{A}, \quad (3)$$

where, \mathbf{R} represents the raindrop residual. This model incorporates the dynamics of raindrops and their impact on the image quality, taking into account the distortion caused by rain streaks and the interaction of raindrops with the scene's atmospheric light.

In addition, the image brightness is reduced using the γ correction method to simulate low light conditions as follows:

$$\mathbf{I} = \mathcal{F}(\mathbf{B}, \gamma), \quad (4)$$

where \mathcal{F} stands for the replacement of the look-up table, and γ indicates the gamma value for luminance correction. This method allows us to create a more realistic representation of images captured in low light scenarios by adjusting the overall brightness and contrast of the scene.

By synthesizing these diverse adverse weather conditions in our dataset, we can effectively evaluate the performance of our proposed MonoTDP model under various challenging scenarios. The data collected for our experiments is illustrated in Figure 3.

3.2 Adaptive Learning Strategy

In this work, we propose a novel adaptive learning strategy comprising a weak constraint encoder and a strong constraint decoder, which are specifically designed to act as a constraint, rather than focusing on image restoration. The primary objective of this module is to facilitate the model's ability to learn and perceive intrinsic features under various adverse conditions.

The weak constraint encoder is devised to understand image features and discern the intricate characteristics of distinct adverse environments by concurrently analyzing intra-patch and normal patch features. This approach assists the model in rectifying inaccurate feature perception under a range of adverse conditions. The



Figure 3: Images under adverse weather conditions, conclude mod fog, thick fog, dense fog, mod rain, heavy rain, dense rain, low light.

strong constraint decoder employs learnable scene penalization queries to detect and penalize the model for incorrect perception across diverse environments. By doing so, it enforces the model to capture the essence of features while suppressing potential errors. The output features from both the encoder and decoder are subsequently fed to the Projection module, which serves to enhance the scene adaptability of MonoTDP. Notably, this learning strategy is only required during the training phase, thus ensuring efficiency and effectiveness in learning essential features in adverse environments.

Given a degraded image I of size $H \times W \times 3$, a common feature extractor is applied to generate low-level features ($\frac{H}{4} \times \frac{W}{4} \times C$). These features are then input into the weak constraint encoder containing SwinBlocks at different stages. We use intra-patch at each stage, where the resolution is reduced to assist the module in learning both coarse and fine contents. Figure 2 provides an overview of the adaptive learning strategy.

The weak constraint encoder is designed to extract multi-level features, thereby generating a hierarchical representation of the input image. During each stage, patch merging is utilized to decrease the resolution, and the merged features are passed on to the subsequent stage. SwinBlocks are then employed to perform feature transformation while maintaining the resolution. A Swin-Block comprises a shifted window-based MSA_{SW} and an MLP, as depicted in Figure 4. Layer Normalization (LN) is applied prior to each MSA_{W} and MLP module, and a residual connection is incorporated following each module. The specific computation process for two consecutive blocks is as follows:

$$\begin{aligned} \hat{z}^l &= \sum_{i=1}^h \omega_i \text{MSA}_{\text{W}} \left(\text{LN} \left(z^{l-1} \right) \right) + z^{l-1}, \\ z^l &= m^l p \left(\text{LN} \left(\hat{z}^l \right) \right) + \hat{z}^l, \\ \hat{z}^{l+1} &= \sum_{i=1}^h \omega_i \text{MSA}_{\text{SW}} \left(\text{LN} \left(z^l \right) \right) + z^l, \\ z^{l+1} &= m^{l+1} p \left(\text{LN} \left(\hat{z}^{l+1} \right) \right) + \hat{z}^{l+1}, \end{aligned} \quad (5)$$

where \hat{z}^l and z^l represent the output of l th $\text{MSA}_{(\text{S})\text{W}}$ and MLP respectively. MSA_{W} and MSA_{SW} denote window based self-attention

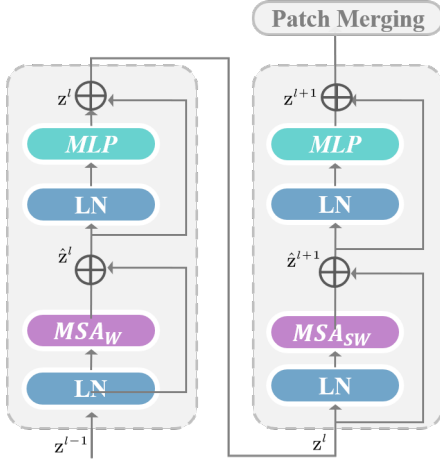


Figure 4: The structure of SwinBlock. It contains two successive Swin Transformer Blocks (notation presented with Eq.(5)). MSA_W and MSA_{SW} are multi-head self attention modules with regular and shifted windowing configurations, respectively. At each stage, we perform a patch merging after SwinBlock except for the last stage.

using traditional and shifted window. The shifted window introduces the connection between diverse parts of the feature map and the computational complexity is only linearly related to the image size. At the same time, intra-patch utilizes a similar SwinBlock as afore-mentioned. Following [31], self-attention is calculated as:

$$\text{Attention}(Q, K, V) = \text{SoftMax}\left(\frac{QK^T}{\sqrt{d}} + B\right)V, \quad (6)$$

where Q, K, V are queries keys and values that have same dimensions. B is relative position bias.

In the strong constraint decoder, scene penalization queries are utilized to output a task feature vector, focusing on the multi-level features from the encoder. The decoder has only one stage but contains multiple blocks. Cross-attention is applied in this module, with K and V taken from the same output features as the last stage of the encoder, and Q being the learnable queries.

The output features of the decoder serve as the weather type task vector and are fused with the features produced by each stage of the encoder. Both output features from the encoder and decoder are then fed to the projection module and are constrained by a *smooth \mathcal{L}_1 loss*. By incorporating weak constraint encoders and strong constraint decoders, the adaptive learning strategy can effectively adapt to diverse adverse environments and improve the precision of 3D object detection in adverse weather conditions. The effectiveness of this learning strategy will be further demonstrated in the subsequent ablation experiments.

3.3 3D Object Detection in Adverse Scenes

Figure 2 shows the framework of our approach, monocular 3D object detection takes an RGB image as input and constructs a 3D bounding box for the object in 3D space. The 3D bounding box consists of the object’s three-dimensional center position (x, y, z) ,

size (h, w, l) and direction Θ that usually refers to the observation angle.

Our monocular 3D detection network obtains the constraint features that are optimized with adaptive learning strategy which are resistant to degrading factors. These features are then forwarded to predict 2D bounding boxes. Concretely, 2D detection backbone is applied to produce high-level deep features, and then these features are aggregated to get deep features with resolution $F \in \mathbf{R}^{\frac{H}{8} \times \frac{W}{8} \times C}$. Subsequently, we apply three 2D detection heads in deep features F to predict 2D heatmap H which has the same size with F , offset O_{2D} , dimension S_{2D} . Afterwards, through using ROI_{Align} in deep feature map with 2D box information, the features of the object are generated whose size is 7×7 . Finally, these features are used in the 3D detection heads to predict the object 3D center offset O_{3d} , 3D size S_{3d} and direction Θ .

Twin Depth Perception. In prevailing 3D object detection approaches, the environmental context encompassing the object is frequently overlooked. As a result, instance depth is predominantly estimated based on the features proximal to the object. This approach leaves depth estimation vulnerable to the adverse effects of various weather conditions, such as the diminished visibility caused by nighttime darkness, the obfuscation induced by fog, and the visual disturbances introduced by rain. These factors can compromise the accuracy of depth estimation.

To mitigate these challenges, we introduce a novel twin depth perception module that concurrently predicts scene depth and object depth. Contrasting with traditional 3D detection heads that directly regress depth, our twin depth perception module fosters interaction between scenes and objects, transcending the limitations of single-object perception. This holistic approach empowers the model to generate more precise inferred depth values.

To clarify, we initially posit that instance depth is composed of two distinct elements: object depth and scene depth. The object depth is obtained by regressing the features of the 7×7 cells after performing RoI Align. Meanwhile, the scene depth is derived from a cross-attention mechanism that considers both the local features of the object and the global feature map, ensuring an accurate depth prediction even under challenging environmental conditions.

For monocular systems, scene depth is heavily contingent upon information from the entire scene, rendering it particularly sensitive to weather condition perception. Estimating scene depth generally demands a comprehensive scene perception. By integrating both scene depth and object depth predictions, our twin depth perception module substantially bolsters the model’s capacity for accurate depth estimation under a wide array of challenging weather conditions, resulting in a more robust and reliable 3D object detection system.

Depth Geometry Uncertainty. Following [29], depth prediction is assumed to be Laplace distribution. For each object depth d_{obj} and the corresponding uncertainty u_{obj} , they follow the Laplace distribution $La(d_{obj}, u_{obj})$. Parallel, the scene depth follows $La(d_{sce}, u_{sce})$, where d_{sce} and u_{sce} denote scene depth and its uncertainty. Accordingly, the final instance depth distribution is $La(d_{ins}, u_{ins})$, where $d_{ins} = d_{obj} + d_{sce}$ and $u_{ins} = \sqrt{u_{obj}^2 + u_{sce}^2}$.

3.4 Loss Functions

Our proposed model is designed to effectively carry out 3D object detection in intricate environments. Throughout the training process, we concurrently compute the losses associated with the adaptive learning strategy and the 3D object detection task.

To accurately capture feature representations under adverse weather conditions, our adaptive learning strategy employs the $smooth_{L_1}$ loss to penalize the incorrect perception of features in challenging scenarios. This loss function is formulated as follows:

$$\mathcal{L}_{smooth_{L_1}} = \begin{cases} 0.5\mathbf{E}^2 & \text{if } |\mathbf{E}| < 1 \\ |\mathbf{E}| - 0.5 & \text{otherwise,} \end{cases} \quad (7)$$

where \mathbf{E} represents the difference between the perceived scene and real scene.

For 3D object detection, the loss function is as the following formula. It can be divided into 2D detection part and 3D detection part. As shown in Figure 2, we use the 2D heatmap H to indicate the rough object center on the image. Its size is $\frac{H}{8} \times \frac{W}{8} \times B$, and B is the number of categories. The 2D offset O_{2D} refers to the residual towards rough 2D centers, and S_{2D} denotes the 2D box height and width. We follow [5] to use loss functions \mathcal{L}_H , $\mathcal{L}_{O_{2d}}$, $\mathcal{L}_{S_{2d}}$.

For the dimensions of the 3D object, we use the typically designed $\mathcal{L}_{S_{3d}}$ and multi-bin to calculate \mathcal{L}_Θ for the prediction of the object observation angle. Furthermore, the position of object is recovered by using the 3D center projection and instance depth. It is achieved by predicting 3D projection offset to the 2D center, and uses smooth L1 loss function $\mathcal{L}_{O_{3d}}$. In addition, the instance depth is decoupled into scene depth and object depth. Like [29], the depth projected by LiDAR is used as the supervision of the scene depth, and the subtraction between the instance depth and the scene depth is used as the supervision of the object depth. The Instance depth is supervised as the sum of scene depth and object depth. The instance depth loss is $\mathcal{L}_{D_{ins}}$ and uncertainty regression loss [24] is applied as:

$$\mathcal{L}_{D_{ins}} = \frac{\sqrt{2}}{u_{vins}} \left\| d_{ins} - d_{ins}^{gt} \right\| + \log(u_{ins}), \quad (8)$$

where u_{ins} denotes the uncertainty and gt is the corresponding label. We set the weight of each loss term to 1.0. The overall loss is:

$$\mathcal{L} = \mathcal{L}_H + \mathcal{L}_{O_{2d}} + \mathcal{L}_{S_{2d}} + \mathcal{L}_{S_{3d}} + \mathcal{L}_\Theta + \mathcal{L}_{O_{3d}} + \mathcal{L}_{D_{ins}}. \quad (9)$$

4 EXPERIMENTS

This section compares the results of our method for 3D object detection in various adverse environments. The experimental datasets are based on KITTI synthetic datasets of rain, fog, and low-light scenes. In which, we measure our model by two sets of comparisons. The first set with the latest monocular 3D object detection model. The second set is compared with the latest defogging model, rain removal model and low-light enhancement model. Our experiments are performed on 4 Nvidia TITAN XP.

4.1 Datasets and Metric

We evaluate the performance of our methods and 5 state-of-the-art under synthetic KITTI 3D dataset, comprising 7,481 images for

each of moderate fog, thick fog, dense fog, moderate rain, heavy rain, dense rain, and low light conditions. as in [6]. Following the methodology of [4], the dataset is partitioned into 3,712 sub-training sets and 3,769 validation sets. Detection outcomes are presented in three levels of difficulty, namely easy, moderate, and hard, with the moderate scores generally utilized for ranking purposes. To assess our performance, we use average precision as the evaluation metric. The 3D bounding box is represented as AP3D $_{R40}$, where R40 signifies 40 recall positions. For the three aforementioned categories, the Intersection over Union (IoU) threshold for cars is set to 0.7.

4.2 Implementation Details

We conduct our experiments using 4 NVIDIA RTX TITAN XP GPUs and a batch size of 8. Our implementation is built upon the PyTorch framework. We train the network for 140 epochs, following the Hierarchical Task Learning (HTL) strategy [24]. The Adam optimizer is employed with an initial learning rate of 1e-5. We apply a linear warm-up strategy to raise the learning rate to 1e-3 during the initial 5 epochs. Subsequently, the learning rate decays at epochs 50 and 80 with a decay rate of 0.1. For the multi-bin orientation θ , we set k to 12. The backbone and head architecture are designed in accordance with [24]. Input images are resized to a resolution of 1280 × 384, with pixel values in the range of [0, 255]. The pixel intensities are then adjusted based on the mean pixel intensity of the entire dataset.

4.3 Comparison with 3D Detection Methods

In this section, we conduct a comprehensive comparison between our proposed method and several state-of-the-art monocular 3D object detection techniques under various adverse weather conditions. These conditions include moderate fog, thick fog, moderate rain, heavy rain, dense rain, and low light. The car category's 3D detection accuracy, denoted by AP3D $_{R40}$, serves as the benchmark for comparison. The results are presented in Table 1.

Our method demonstrates significant performance improvements across different weather conditions. Under heavy rain conditions, our approach achieves gains of 1.66%, 0.98%, and 0.87% on the easy, moderate, and hard settings, respectively. Similarly, under thick fog conditions, our method obtains 1.66%, 0.98%, and 0.87% gains for the same settings. Furthermore, when evaluated on the thick fog dataset, our method outperforms GUPNet by 3.33%, 2.04%, and 1.78% in terms of 3D detection under the three settings at a 0.7 IoU threshold. Additionally, our MonoTDP method substantially surpasses DID-M3D and MonoDLE in the low light dataset, with improvements of 0.91% and 3.71% AP3D $_{R40}$ under moderate settings. This result serves to validate the effectiveness of our approach.

The superior performance of our method can be attributed to the integration of environmental constraints, as well as the innovative twin depth perception module that concurrently predicts scene depth and object depth. By incorporating both local and global features, our method effectively captures the nuances of various weather conditions and enables more accurate depth estimation. Consequently, our method demonstrates exceptional results across a range of rain, fog, and low light conditions, underscoring its robustness and applicability in diverse real-world scenarios.

Table 1: Comparison of the latest 3D object detection methods on the moderate fog, thick fog, moderate rain, heavy rain, dense rain and low light dataset based on AP_{3D} of the car category. All methods have been retrained on the respective environmental datasets. Red and Blue correspond to the first and second best results, respectively. Quantitative results substantiate that our method achieves state-of-the-art performance.

| Methods | Venue | Mod. Fog | | | Thick Fog | | | Mod. Rain | | | Heavy Rain | | | Dense Rain | | | Low Light | | |
|----------------|---------------|--------------|--------------|--------------|--------------|--------------|--------------|--------------|--------------|--------------|--------------|--------------|--------------|--------------|--------------|--------------|--------------|--------------|--------------|
| | | Easy | Mod. | Hard | Easy | Mod. | Hard | Easy | Mod. | Hard | Easy | Mod. | Hard | Easy | Mod. | Hard | Easy | Mod. | Hard |
| SMOKE | <i>CVPR20</i> | 8.86 | 5.98 | 4.53 | 5.10 | 3.31 | 2.28 | 7.33 | 5.24 | 4.03 | 5.97 | 3.78 | 2.77 | 5.64 | 3.88 | 3.21 | 5.48 | 4.03 | 3.49 |
| MonoFLEX | <i>CVPR21</i> | 19.97 | 14.11 | 11.86 | 18.37 | 13.28 | 10.57 | 17.21 | 12.94 | 11.55 | 16.99 | 11.83 | 10.12 | 15.35 | 12.14 | 10.38 | 10.43 | 8.32 | 7.75 |
| MonoDLE | <i>CVPR21</i> | 14.77 | 12.15 | 10.02 | 17.35 | 12.89 | 11.27 | 15.65 | 13.34 | 12.33 | 15.64 | 12.63 | 11.13 | 14.94 | 11.20 | 9.78 | 14.69 | 11.99 | 10.60 |
| GUPNet | <i>ICCV21</i> | 21.06 | 15.02 | 12.34 | 19.91 | 14.24 | 11.57 | 19.69 | 14.24 | 12.36 | 17.36 | 12.95 | 10.76 | 16.71 | 12.40 | 10.64 | 9.84 | 6.36 | 5.09 |
| DID-M3D | <i>ECCV22</i> | 22.75 | 15.52 | 12.61 | 22.19 | 15.96 | 12.86 | 22.42 | 15.30 | 12.43 | 21.40 | 14.79 | 12.05 | 20.56 | 14.07 | 11.88 | 21.92 | 14.79 | 12.10 |
| DEVIANT | <i>ECCV22</i> | 22.74 | 15.92 | 13.16 | 22.90 | 16.11 | 13.25 | 22.35 | 15.99 | 12.45 | 20.18 | 13.93 | 11.96 | 20.20 | 13.85 | 12.26 | 22.40 | 15.16 | 12.33 |
| HomoLoss | <i>CVPR22</i> | 14.31 | 12.27 | 11.12 | 19.32 | 13.26 | 11.51 | 18.23 | 13.19 | 12.56 | 17.69 | 13.01 | 12.23 | 16.33 | 13.40 | 10.76 | 15.88 | 13.89 | 11.42 |
| CubeR-CNN | <i>CVPR23</i> | 21.11 | 14.97 | 12.55 | 20.81 | 14.77 | 12.12 | 20.37 | 14.14 | 12.38 | 22.36 | 13.67 | 11.11 | 19.17 | 13.54 | 10.99 | 20.11 | 14.37 | 11.89 |
| MonoTDP | - | 23.13 | 16.03 | 13.19 | 23.24 | 16.28 | 13.35 | 23.08 | 16.01 | 12.98 | 23.06 | 15.77 | 12.92 | 21.31 | 15.40 | 12.52 | 22.55 | 15.70 | 12.80 |
| Improvement | | +0.38 | +0.11 | +0.03 | +0.34 | +0.17 | +0.10 | +0.66 | +0.02 | +0.53 | +1.66 | +0.98 | +0.87 | +0.75 | +1.33 | +0.26 | +0.15 | +0.54 | +0.49 |

Table 2: Comparison of our proposed method with the combinations of our base 3D detection network and popular enhancement models under various challenging conditions for the car category, evaluated using AP_{R40} at IoU threshold of 0.7. We compared our method under thick fog with dehazing models, under heavy rain with deraining models, and under low light with low-light enhancement models, all combined with our base 3D detection model.

| Scene | Methods | Venue | Car 3D@IOU=0.7 | | |
|------------|---------|---------------|----------------|--------------|--------------|
| | | | Easy | Mod. | Hard |
| Thick Fog | Trans | <i>CVPR22</i> | 22.95 | 16.03 | 13.21 |
| | MSBDN | <i>CVPR20</i> | 20.11 | 14.14 | 11.55 |
| | GCA | <i>WACV19</i> | 21.21 | 14.08 | 12.49 |
| | DCPDN | <i>CVPR18</i> | 19.97 | 13.25 | 11.34 |
| | Ours | - | 23.13 | 16.03 | 12.95 |
| Heavy Rain | Trans | <i>CVPR22</i> | 20.29 | 13.89 | 11.67 |
| | RESCAN | <i>ECCV18</i> | 20.06 | 13.81 | 10.99 |
| | VRGNet | <i>CVPR21</i> | 21.55 | 12.98 | 11.01 |
| | PRENet | <i>CVPR19</i> | 20.11 | 13.34 | 10.67 |
| | Ours | - | 23.06 | 15.77 | 12.92 |
| Low Light | Trans | <i>CVPR22</i> | 14.7 | 10.53 | 9.18 |
| | SCI | <i>CVPR22</i> | 19.88 | 14.12 | 10.68 |
| | IAT | <i>BMVC22</i> | 19.84 | 13.59 | 10.94 |
| | SID | <i>CVPR18</i> | 17.78 | 12.21 | 10.32 |
| | Ours | - | 22.55 | 15.70 | 12.82 |

4.4 Comparison with Restoration Methods

In this section, we extend our comparison to evaluate the performance of our base 3D detection network combined with various image restoration techniques under different adverse weather conditions. We aim to demonstrate the effectiveness of our adaptive learning strategy against the top-performing defog, rain removal, and low-light enhancement models in thick fog, heavy rain, and low-light environments, respectively. TransWeather is trained in

these three weather conditions since it is designed to adapt to various weather scenarios. Other methods are trained under specific environments tailored to their corresponding effects.

As shown in the table 2, the performance comparison between our method and several other methods in dense fog, heavy rain, and low light environments is shown. Among them, the performance of MonoTDP is comparable to TransWeather in dense fog, but shows significant improvement under heavy rain conditions. Under low light conditions it has significantly improved by 7.85%, 5.17%, and 3.64% under the three settings of easy, mod, and hard, respectively. In addition, our method is also significantly superior to all other task specific methods. For example, under dense fog conditions, our method improved by 3.13%, 2.14%, and 1.80% compared to MSBDN under three different settings, respectively. There is also a significant improvement compared to GCA. In heavy rain environments, our method has improved by 1.51%, 2.79%, and 1.91% compared to VRGNet in three settings, and has greater improvement compared to RESCAN. Under low light conditions, in addition to TransWeather, MonoTDP also performs better than SCI and IAT. It can be observed easily from the data that our method has achieved the best performance under various conditions, whether in easy, mod, or hard metrics, which is superior to existing methods. It significantly improves the accuracy and robustness of image restoration in harsh environments.

In summary, our proposed method not only attains state-of-the-art accuracy in harsh environments when compared to the leading 3D object detection techniques, but it also outperforms existing image restoration methods. This result highlights the robustness and adaptability of our approach in diverse and challenging scenarios.

4.5 Ablation Study

To investigate how each module in MonoTDP enhances 3D object detection, we randomly selected one seventh of medium rain, heavy rain, dense rain, thin fog, thick fog, dense fog, and low light to obtain a mixed dataset, and then tested each module on this mixed dataset. The results are shown in Table 3.

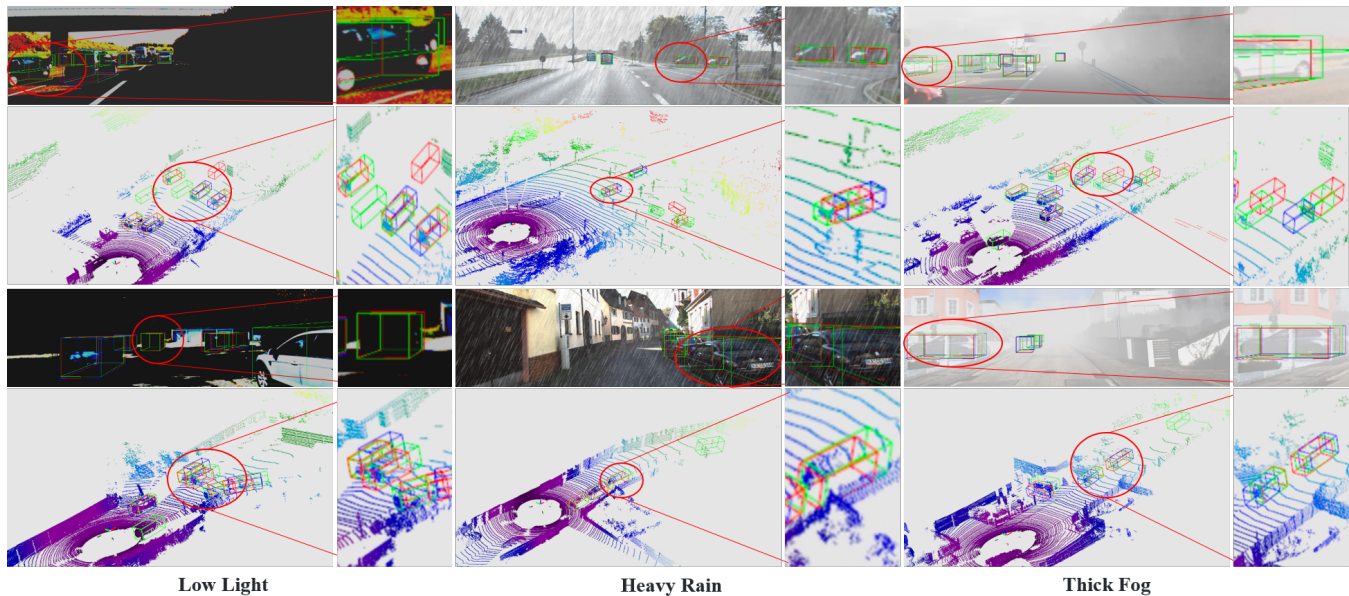


Figure 5: Qualitative results on the validation set of hybrid dataset which contain all types of weather. These results are based on method trained on the train set. Three columns show the 3D target detection results under different scenes. We use green, red, blue boxes to denote ground-truth, our predictions and predictions of GUPNet(One of the most popular 3D Detection Model) respectively. LiDAR signals are only used for visualization.

Table 3: Ablation study for the components of our method. Results are reported on hybrid datasets contain fog, rain, low light conditions of diverse grees.

| | WCE | SCD | D_{obj} | D_{sce} | 3D@IoU=0.7 | | |
|-----|--------------|--------------|--------------|--------------|-----------------------|-----------------------|-----------------------|
| | | | | | Easy \uparrow | Mod. \uparrow | Hard \uparrow |
| (a) | - | - | - | - | 18.53 | 13.09 | 10.89 |
| (b) | \checkmark | - | - | - | 19.12 \uparrow 0.59 | 14.43 \uparrow 1.34 | 11.74 \uparrow 0.85 |
| (c) | \checkmark | \checkmark | - | - | 20.35 \uparrow 1.82 | 14.86 \uparrow 1.77 | 12.11 \uparrow 1.22 |
| (e) | - | - | \checkmark | - | 20.86 \uparrow 2.33 | 14.11 \uparrow 1.02 | 11.86 \uparrow 0.97 |
| (f) | - | - | \checkmark | \checkmark | 21.54 \uparrow 3.01 | 14.25 \uparrow 1.16 | 12.01 \uparrow 1.12 |
| (g) | \checkmark | - | \checkmark | \checkmark | 22.18 \uparrow 3.65 | 14.77 \uparrow 1.68 | 12.12 \uparrow 1.23 |
| (h) | \checkmark | \checkmark | \checkmark | \checkmark | 23.22 \uparrow 4.69 | 15.55 \uparrow 2.46 | 12.31 \uparrow 1.42 |

We evaluate the effectiveness of our adaptive learning strategy which is divided into two parts: Weak Constraint Encoder (WCE) and Strong Constraint Decoder (SCD). We conduct experiments to evaluate the impact of each part on the overall performance of our 3D object detection system.

First, we examine the WCE’s contribution by comparing settings (a \rightarrow b) and (f \rightarrow g). The results demonstrate that the WCE consistently improves the overall performance by 0.34% for (a \rightarrow b) and 0.52% for (f \rightarrow g) under moderate settings. This highlights the WCE’s ability to effectively and stably enhance the 3D object detection task.

Next, we assess the SCD’s effectiveness through experiments (b \rightarrow c) and (g \rightarrow h). The observed performance improvement indicates that the SCD is also a crucial component of our learning

strategy. Both parts of the module prove to be indispensable for optimal performance.

To further investigate the role of our twin depth perception module, we conduct two sets of control experiments (b \rightarrow g and c \rightarrow h). The significant improvement observed in these experiments demonstrates that the combination of object depth (D_{obj}) and scene depth (D_{sce}) enhances the model’s ability to comprehend instance depth.

In particular, the experiments (e \rightarrow f and g \rightarrow h) reveal that the scene depth design allows the model to obtain more accurate depth estimates across various environments, thereby improving 3D object detection performance. The experimental results conclusively demonstrate the effectiveness of our proposed method.

4.6 Qualitative Results

A close examination of the information presented in Figure 5 reveals the superior performance of our proposed method, MonoTDP, compared to the current state-of-the-art approach, GUPNet, in three distinct environments: low light, rainy, and foggy conditions. In low light scenarios, where the environment is comparatively dark, GUPNet tends to miss objects, whereas MonoTDP demonstrates higher accuracy in recognizing the majority of images. Under rainy conditions, GUPNet struggles to correctly identify numerous objects due to rain-induced obstructions. In contrast, our method exhibits minimal target misidentification, thereby addressing a significant limitation of GUPNet. In foggy situations characterized by low visibility, GUPNet’s recognition results often deviate considerably from the correct outcomes, leading to inaccurate object detection. Conversely, MonoTDP accurately identifies nearly all objects. These

observations highlight the considerable advantages of our method over other optimal approaches, emphasizing its resilience against environmental challenges. MonoTDP effectively tackles issues, such as texture loss, rain streak occlusions, and impaired visibility, which are prevalent in real-world 3D object detection tasks.

5 CONCLUSION

In this study, we introduce MonoTDP, a monocular 3D object detection model adept at perceiving twin depth and demonstrating exceptional performance in an array of challenging environments, including fog, rain, and low-light conditions. Incorporating an adaptive learning strategy and a twin depth perception module, our model enhances the accuracy of 3D object detection, even under adverse circumstances. MonoTDP effectively utilizes the adaptive learning strategy to regularize the model, enabling it to adapt to inclement weather conditions and perceive features across diverse scenes. Simultaneously, the model estimates both scene depth and object depth, thus rendering the depth prediction process scene-aware. This innovative approach substantially advances the practical applicability of monocular 3D object detection models. Extensive experimental results attest to the superiority of our proposed method over state-of-the-art approaches, both qualitatively and quantitatively, across various adverse environments.

REFERENCES

- [1] Garrick Brazil and Xiaoming Liu. 2019. M3d-rpn: Monocular 3d region proposal network for object detection. In *Proceedings of the IEEE/CVF International Conference on Computer Vision*. 9287–9296.
- [2] Bolun Cai, Xiangmin Xu, Kui Jia, Chunmei Qing, and Dacheng Tao. 2016. Dehazenet: An end-to-end system for single image haze removal. *IEEE Transactions on Image Processing* 25, 11 (2016), 5187–5198.
- [3] Chen Chen, Qifeng Chen, Jia Xu, and Vladlen Koltun. 2018. Learning to see in the dark. In *Proceedings of the IEEE conference on computer vision and pattern recognition*. 3291–3300.
- [4] Xiaozhi Chen, Kaustav Kundu, Ziyu Zhang, Huimin Ma, Sanja Fidler, and Raquel Urtasun. 2016. Monocular 3d object detection for autonomous driving. In *Proceedings of the IEEE conference on computer vision and pattern recognition*. 2147–2156.
- [5] Kaiwen Duan, Song Bai, Lingxi Xie, Honggang Qi, Qingming Huang, and Qi Tian. 2019. Centernet: Keypoint triplets for object detection. In *Proceedings of the IEEE/CVF international conference on computer vision*. 6569–6578.
- [6] Andreas Geiger, Philip Lenz, and Raquel Urtasun. 2012. Are we ready for autonomous driving? the kitti vision benchmark suite. In *2012 IEEE conference on computer vision and pattern recognition*. 3354–3361.
- [7] Kaiming He, Georgia Gkioxari, Piotr Dollár, and Ross Girshick. 2017. Mask r-cnn. In *Proceedings of the IEEE international conference on computer vision*. 2961–2969.
- [8] Peixuan Li and Huaici Zhao. 2021. Monocular 3d detection with geometric constraint embedding and semi-supervised training. *IEEE Robotics and Automation Letters* 6, 3 (2021), 5565–5572.
- [9] Peixuan Li, Huaici Zhao, Pengfei Liu, and Feidao Cao. 2020. Rtm3d: Real-time monocular 3d detection from object keypoints for autonomous driving. In *European Conference on Computer Vision*. 644–660.
- [10] Ruoteng Li, Loong-Fah Cheong, and Robby T Tan. 2019. Heavy rain image restoration: Integrating physics model and conditional adversarial learning. In *Proceedings of the IEEE/CVF Conference on Computer Vision and Pattern Recognition*. 1633–1642.
- [11] Runde Li, Jinshan Pan, Zechao Li, and Jinhui Tang. 2018. Single image dehazing via conditional generative adversarial network. In *Proceedings of the IEEE Conference on Computer Vision and Pattern Recognition*. 8202–8211.
- [12] Ruoteng Li, Robby T Tan, and Loong-Fah Cheong. 2020. All in one bad weather removal using architectural search. In *Proceedings of the IEEE/CVF conference on computer vision and pattern recognition*. 3175–3185.
- [13] Jingyun Liang, Jie Zhang Cao, Guolei Sun, Kai Zhang, Luc Van Gool, and Radu Timofte. 2021. Swinir: Image restoration using swin transformer. In *Proceedings of the IEEE/CVF International Conference on Computer Vision*. 1833–1844.
- [14] Jinyuan Liu, Xin Fan, Zhanbo Huang, Guanyao Wu, Risheng Liu, Wei Zhong, and Zhongxuan Luo. 2022. Target-aware dual adversarial learning and a multi-scenario multi-modality benchmark to fuse infrared and visible for object detection. In *Proceedings of the IEEE/CVF Conference on Computer Vision and Pattern Recognition*. 5802–5811.
- [15] Jinyuan Liu, Xin Fan, Ji Jiang, Risheng Liu, and Zhongxuan Luo. 2021. Learning a deep multi-scale feature ensemble and an edge-attention guidance for image fusion. *IEEE Transactions on Circuits and Systems for Video Technology* 32, 1 (2021), 105–119.
- [16] Risheng Liu, Xin Fan, Minjun Hou, Zhiying Jiang, Zhongxuan Luo, and Lei Zhang. 2018. Learning aggregated transmission propagation networks for haze removal and beyond. *IEEE transactions on neural networks and learning systems* 30, 10 (2018), 2973–2986.
- [17] Risheng Liu, Minjun Hou, Jinyuan Liu, Xin Fan, and Zhongxuan Luo. 2019. Compounded layer-prior unrolling: A unified transmission-based image enhancement framework. In *2019 IEEE International Conference on Multimedia and Expo (ICME)*. IEEE, 538–543.
- [18] Risheng Liu, Zhiying Jiang, Xin Fan, and Zhongxuan Luo. 2019. Knowledge-driven deep unrolling for robust image layer separation. *IEEE transactions on neural networks and learning systems* 31, 5 (2019), 1653–1666.
- [19] Risheng Liu, Zhiying Jiang, Long Ma, Xin Fan, Haojie Li, and Zhongxuan Luo. 2018. Deep layer prior optimization for single image rain streaks removal. In *2018 IEEE International Conference on Acoustics, Speech and Signal Processing (ICASSP)*. IEEE, 1408–1412.
- [20] Risheng Liu, Shiqi Li, Jinyuan Liu, Long Ma, Xin Fan, and Zhongxuan Luo. 2020. Learning hadamard-product-propagation for image dehazing and beyond. *IEEE Transactions on Circuits and Systems for Video Technology* 31, 4 (2020), 1366–1379.
- [21] Risheng Liu, Jinyuan Liu, Zhiying Jiang, Xin Fan, and Zhongxuan Luo. 2020. A bilevel integrated model with data-driven layer ensemble for multi-modality image fusion. *IEEE Transactions on Image Processing* 30 (2020), 1261–1274.
- [22] Zechen Liu, Zizhang Wu, and Roland Tóth. 2020. Smoke: Single-stage monocular 3d object detection via keypoint estimation. In *Proceedings of the IEEE/CVF Conference on Computer Vision and Pattern Recognition Workshops*. 996–997.
- [23] Kin Gwn Lore, Adedotun Akintayo, and Soumik Sarkar. 2017. LLNet: A deep auto-encoder approach to natural low-light image enhancement. *Pattern Recognition* 61 (2017), 650–662.

- [24] Yan Lu, Xinzhu Ma, Lei Yang, Tianzhu Zhang, Yating Liu, Qi Chu, Junjie Yan, and Wanli Ouyang. 2021. Geometry uncertainty projection network for monocular 3d object detection. In *Proceedings of the IEEE/CVF International Conference on Computer Vision*. 3111–3121.
- [25] Feifan Lv, Feng Lu, Jianhua Wu, and Chongsoon Lim. 2018. MBLEN: Low-Light Image/Video Enhancement Using CNNs. In *BMVC*, Vol. 220. 4.
- [26] Xinzhu Ma, Yinmin Zhang, Dan Xu, Dongzhan Zhou, Shuai Yi, Haojie Li, and Wanli Ouyang. 2021. Delving into localization errors for monocular 3d object detection. In *Proceedings of the IEEE/CVF Conference on Computer Vision and Pattern Recognition*. 4721–4730.
- [27] Fabian Manhardt, Wadim Kehl, and Adrien Gaidon. 2019. Roi-10d: Monocular lifting of 2d detection to 6d pose and metric shape. In *Proceedings of the IEEE/CVF Conference on Computer Vision and Pattern Recognition*. 2069–2078.
- [28] Arsalan Mousavian, Dragomir Anguelov, John Flynn, and Jana Kosecka. 2017. 3d bounding box estimation using deep learning and geometry. In *Proceedings of the IEEE conference on Computer Vision and Pattern Recognition*. 7074–7082.
- [29] Liang Peng, Xiaopei Wu, Zheng Yang, Haifeng Liu, and Deng Cai. 2022. DID-M3D: Decoupling Instance Depth for Monocular 3D Object Detection. In *European Conference on Computer Vision*. 71–88.
- [30] Yuhui Qian, Shijie Deng, Yixin Chen, and Hui Ji. 2019. Deep learning for seeing through window with raindrops. In *Proceedings of the IEEE/CVF International Conference on Computer Vision*. 2463–2471.
- [31] Colin Raffel, Noam Shazeer, Adam Roberts, Katherine Lee, Sharan Narang, Michael Matena, Yanqi Zhou, Wei Li, Peter J Liu, et al. 2020. Exploring the limits of transfer learning with a unified text-to-text transformer. *J. Mach. Learn. Res.* 21, 140 (2020), 1–67.
- [32] Wenqi Ren, Sifei Liu, Lin Ma, Qianqian Xu, Xiangyu Xu, Xiaochun Cao, Junping Du, and Ming-Hsuan Yang. 2019. Low-light image enhancement via a deep hybrid network. *IEEE Transactions on Image Processing* 28, 9 (2019), 4364–4375.
- [33] Liang Shen, Zihan Yue, Fan Feng, Quan Chen, Shihao Liu, and Jie Ma. 2017. Msr-net: Low-light image enhancement using deep convolutional network. *arXiv preprint arXiv:1711.02488* (2017).
- [34] Hualian Sheng, Sijia Cai, Na Zhao, Bing Deng, Jianqiang Huang, Xian-Sheng Hua, Min-Jian Zhao, and Gim Hee Lee. 2022. Rethinking IoU-based Optimization for Single-stage 3D Object Detection. In *Computer Vision—ECCV 2022: 17th European Conference, Tel Aviv, Israel, October 23–27, 2022, Proceedings, Part IX*. Springer, 544–561.
- [35] Li Tao, Chuang Zhu, Guoqing Xiang, Yuan Li, Huizhu Jia, and Xiaodong Xie. 2017. LLCNN: A convolutional neural network for low-light image enhancement. In *2017 IEEE Visual Communications and Image Processing (VCIP)*. 1–4.
- [36] Zhi Tian, Chunhua Shen, Hao Chen, and Tong He. 2019. Fcos: Fully convolutional one-stage object detection. In *Proceedings of the IEEE/CVF international conference on computer vision*. 9627–9636.
- [37] Hong Wang, Qi Xie, Qian Zhao, and Deyu Meng. 2020. A model-driven deep neural network for single image rain removal. In *Proceedings of the IEEE/CVF Conference on Computer Vision and Pattern Recognition*. 3103–3112.
- [38] Tianyu Wang, Xin Yang, Ke Xu, Shaozhe Chen, Qiang Zhang, and Rynson WH Lau. 2019. Spatial attentive single-image deraining with a high quality real rain dataset. In *Proceedings of the IEEE/CVF Conference on Computer Vision and Pattern Recognition*. 12270–12279.
- [39] Tai Wang, Xinge Zhu, Jiangmiao Pang, and Dahua Lin. 2021. Fcos3d: Fully convolutional one-stage monocular 3d object detection. In *Proceedings of the IEEE/CVF International Conference on Computer Vision*. 913–922.
- [40] Yan Wang, Wei-Lun Chao, Divyansh Garg, Bharath Hariharan, Mark Campbell, and Kilian Q Weinberger. 2019. Pseudo-lidar from visual depth estimation: Bridging the gap in 3d object detection for autonomous driving. In *Proceedings of the IEEE/CVF Conference on Computer Vision and Pattern Recognition*. 8445–8453.
- [41] Qiangeng Xu, Yin Zhou, Weiyue Wang, Charles R Qi, and Dragomir Anguelov. 2021. Spg: Unsupervised domain adaptation for 3d object detection via semantic point generation. In *Proceedings of the IEEE/CVF International Conference on Computer Vision*. 15446–15456.
- [42] Honghui Yang, Zili Liu, Xiaopei Wu, Wenxiao Wang, Wei Qian, Xiaofei He, and Deng Cai. 2022. Graph R-CNN: Towards Accurate 3D Object Detection with Semantic-Decorated Local Graph. In *Computer Vision—ECCV 2022: 17th European Conference, Tel Aviv, Israel, October 23–27, 2022, Proceedings, Part VIII*. Springer, 662–679.
- [43] Wenhan Yang, Robby T Tan, Jiashi Feng, Zongming Guo, Shuicheng Yan, and Jiaying Liu. 2019. Joint rain detection and removal from a single image with contextualized deep networks. *IEEE transactions on pattern analysis and machine intelligence* 42, 6 (2019), 1377–1393.
- [44] Syed Waqas Zamir, Aditya Arora, Salman Khan, Munawar Hayat, Fahad Shahbaz Khan, Ming-Hsuan Yang, and Ling Shao. 2020. Learning enriched features for real image restoration and enhancement. In *European Conference on Computer Vision*. 492–511.
- [45] He Zhang and Vishal M Patel. 2018. Densely connected pyramid dehazing network. In *Proceedings of the IEEE conference on computer vision and pattern recognition*. 3194–3203.
- [46] He Zhang and Vishal M Patel. 2018. Density-aware single image de-raining using a multi-stream dense network. In *Proceedings of the IEEE conference on computer vision and pattern recognition*. 695–704.
- [47] He Zhang, Vishwanath Sindagi, and Vishal M Patel. 2019. Image de-raining using a conditional generative adversarial network. *IEEE transactions on circuits and systems for video technology* 30, 11 (2019), 3943–3956.
- [48] Jingang Zhang, Wenqi Ren, Shengdong Zhang, He Zhang, Yunfeng Nie, Zhe Xue, and Xiaochun Cao. 2021. Hierarchical density-aware dehazing network. *IEEE Transactions on Cybernetics* (2021).
- [49] Yanfu Zhang, Li Ding, and Gaurav Sharma. 2017. Hazerd: an outdoor scene dataset and benchmark for single image dehazing. In *2017 IEEE international conference on image processing (ICIP)*. 3205–3209.
- [50] Yunpeng Zhang, Jiwen Lu, and Jie Zhou. 2021. Objects are different: Flexible monocular 3d object detection. In *Proceedings of the IEEE/CVF Conference on Computer Vision and Pattern Recognition*. 3289–3298.
- [51] Yonghua Zhang, Jiawan Zhang, and Xiaojie Guo. 2019. Kindling the darkness: A practical low-light image enhancer. In *Proceedings of the 27th ACM international conference on multimedia*. 1632–1640.
- [52] Yin Zhou and Oncel Tuzel. 2018. Voxelnet: End-to-end learning for point cloud based 3d object detection. In *Proceedings of the IEEE conference on computer vision and pattern recognition*. 4490–4499.
- [53] Xizhou Zhu, Weijie Su, Lewei Lu, Bin Li, Xiangang Wang, and Jifeng Dai. 2020. Deformable detr: Deformable transformers for end-to-end object detection. *arXiv preprint arXiv:2010.04159* (2020).